Compact All-Fiber Polarization Coherent Lidar Based on a Polarization Modulator

Zhongyang Xu, Hongxiang Zhang, Kai Chen, and Shilong Pan, *Senior Member, IEEE*

***Abstract*— A compact all-fiber polarization coherent Lidar is demonstrated to simultaneously measure the velocity and depolarization ratio. In the Lidar system, a dual-polarization light beam is generated in a polarization modulator (PolM). The light beam consists of a linearly polarized optical carrier and an optical sideband with an orthogonal polarization state. If the light is depolarized, the polarization directions of the optical carrier and the sideband are rotated. Both of them can be detected along the polarization direction of the original optical carrier. In the receiver, the backscattered light along the polarization direction of the original optical carrier is selected and beats with a frequency-shifted optical local oscillator (LO) signal at a photodetector. A beat signal consisting of two single-frequency components will be generated. The velocity is extracted from the frequencies of the two single-frequency components, while the depolarization ratio can be extracted from the intensity ratio of the two single-frequency components. An experiment is carried out, in which a 159-MHz signal is applied to the PolM, and an 80-MHz signal is used to produce the frequency-shifted optical LO. Two single-frequency signals at 80 and 79 MHz are generated at the receiver and used to simultaneously measure the velocity and depolarization of a target in real time.**

***Index Terms*— Depolarization effect, heterodyne, laser Doppler velocimetry, Lidar, polarization modulator (PolM).**

I. Introduction

SINCE the early demonstrations in the 1960s, various Lidar systems have been developed for applications in areas such as ranging [1], meteorological observation [2], remote sensing [3], 3-D imaging [4], and automatic drive [5]. Especially, Lidars are widely used for atmospheric characterizations in the meteorological observation area. Many atmospheric parameters, including the wind velocity [6], backscattered coefficient [7], absorption coefficient [8], type of aerosols [9], and temperature [10] are measured using different Lidars. A polarization Lidar is a type of Lidar that measures the depolarization ratio of the backscattered light to determine the type of aerosols [11], since the light backscattered from polyhedral ice crystals is more depolarized than that from spherical water droplets [12]. By analyzing the polarization states of the backscattered light, the polarization Lidar has been widely applied in appilcations to discriminate between the ice and water in clouds and to characterize vegetation [13], soils [14], and insects [15].

In the polarization Lidar system, the light along two orthogonal polarization directions has to be separately measured so that the depolarization ratio can be extracted [16]. A direct approach is to use a polarization beam splitter (PBS) and two detectors to separately measure the light in two different channels [17]. However, it requires calibration of the differences between the two detectors. Another approach is to measure the orthogonally polarized light with only one detector, in which the lights along two orthogonal polarization directions are alternately measured in different time slots [18], [19]. For example, the polarization of the incident light can be periodically alternated by a rotating polarization filter in front of the receiver. Hence, the lights along the copolarization and the cross-polarization directions are separately measured [18]. The polarization state of light can also be changed in the transmitter by an actively controlled liquid crystal retarder [19]. As a result, the linearly polarized light and circularly polarized light are alternately transmitted so that the depolarization ratio can be measured. Nevertheless, free-space optical components including a liquid crystal retarder plate and a PBS are used in the systems, which make the system complicated. Moreover, in [18] and [19], the lights along the two polarization directions are measured in different time slots which makes it difficult to measure the rapid changes in the atmosphere.

Recently, all-fiber Lidar systems have been developed and widely used for meteorological observations due to the advantages in terms of compactness, robustness, and low cost [20]–[23]. Especially, for a polarization Lidar, mature all-fiber polarization-diversity front-ends and receivers make it easier to change the polarization state of light. In [22], the polarization direction of light is switched by a polarization-diversity optical front-end so that the light along the p-polarization and s-polarization directions are alternately transmitted. The polarization-diversity receiver can also be used to build an all-fiber polarization Lidar [23]. A time-division multiplexing module is used to introduce a time delay between the copolarization and the cross-polarization backscattered lights so that they are detected in different time slots. Due to the all-fiber coherent detection, both Lidar systems have the feasibility to measure the velocity of the target. However, the copolarized and cross-polarized light are still measured in different time slots which makes it impossible to measure the rapid changes in the atmosphere. In

Manuscript received October 3, 2018; revised April 4, 2019; accepted May 22, 2019. Date of publication June 20, 2019; date of current version April 7, 2020. This work was supported in part by the NSFC Program under Grant 61605190 and Grant 61527820 and in part by the Fundamental Research Funds for Central Universities. The Associate Editor coordinating the review process was Branislav Djokic. *(Corresponding author: Shilong Pan.)*

The authors are with the Key Laboratory of Radar Imaging and Microwave Photonics, Ministry of Education, Nanjing University of Aeronautics and Astronautics, Nanjing 210016, China (e-mail: pans@nuaa.edu.cn).

Color versions of one or more of the figures in this article are available online at http://ieeexplore.ieee.org.

Digital Object Identifier 10.1109/TIM.2019.2921053

addition, the two Lidar systems need either the polarization-diversity optical front-end or polarization-diversity receiver, which make the architecture sophisticated.

In this paper, we propose and demonstrate a compact all-fiber coherent polarization Lidar system to simultaneously measure the velocity and depolarization ratio of a target. The key component of the proposed system is a polarization modulator (PolM). If a linearly polarized optical carrier with its polarization direction at an angle of 45° to the principal axes of the PolM is injected, the PolM will output a dual-polarization light consisting of the residual carrier and an optical sideband with orthogonal polarization states. In the receiver, a frequency-shifted optical local oscillator (LO) signal is produced via modulating the optical carrier with an acousto-optic modulator (AOM). The optical LO is combined with the backscattered light and directed to a balanced photodetector (BPD). If the light is depolarized, both the optical carrier and the sideband are present along the polarization direction of the original optical carrier. A beat signal consisting of two single-frequency components will be generated. The frequencies of the two single-frequency components can be used to estimate the velocity. Since the optical carrier and the optical sideband respectively represent the copolarization and cross-polarization components, the intensity ratio of them can be applied to obtain the depolarization ratio. An experiment is carried out. The velocity and depolarization ratio of the light backscattered by a moving mirror is simultaneously measured. Since the lights along the two polarizations are concurrent, the proposed polarization Lidar can implement real-time measurement without using any polarization-switching device. Moreover, if another BPD is adopted, both the optical rotation effect [24] and the depolarization effect can be distinguished.

II. Principle and System

Fig. 1 shows the schematic of the proposed all-fiber polarization coherent Lidar system, in which a dual-polarization light beam is generated by a PolM. A continuous-wave (CW) light from a laser diode (LD) is first split by an optical coupler (OC). One part of the light is modulated in the PolM by a single-frequency signal, while the other part is frequency-shifted by an AOM and serves as the optical LO. The PolM is a special phase modulator, in which lights along the TE and TM modes are modulated with opposite phase modulation indices [25]. If the incident light is oriented with an angle of 45° to one principal axis of the PolM, two complementary phase-modulated signals can be generated along the principal axes of the PolM. In this condition, the even order optical sidebands of the modulated light are along the +45° direction, while the odd order sidebands are along the −45° direction [26], [27]. If the axes along the ±45° directions are chosen as the coordinates, the electrical field of the dual-polarization light beam can be written as

$$\mathbf{E}_A(t) \propto \frac{A_{\text{in}}}{\sqrt{2}} e^{j\omega_c t} \begin{bmatrix} J_0(\beta) \\ J_1(\beta)\left(e^{j\omega_e t} - e^{-j\omega_e t}\right) \end{bmatrix} \tag{1}$$

where A_{in} is the magnitude of the input light, ω_c and ω_e are the angular frequencies of the optical carrier and the single-frequency modulation signal, β is the modulation index,

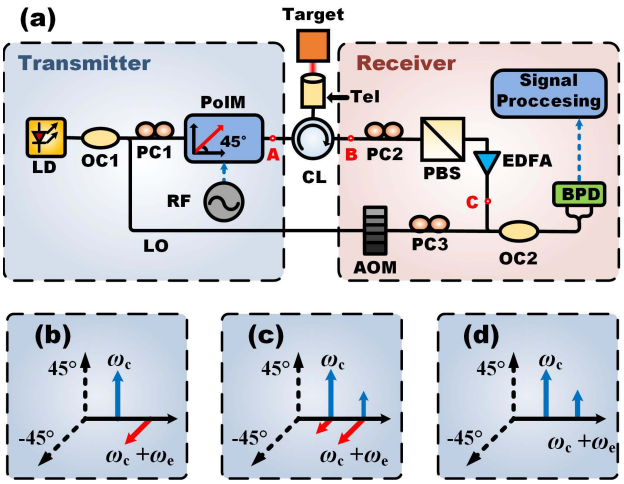

Fig. 1. (a) Experiment setup of the proposed all-fiber polarization coherent Lidar system. (b)–(d) Optical spectra at the point A, B, and C shown in (a). LD: laser diode; OC: optical coupler; PC: polarization controller; PolM: polarization modulator; CL: circulator; Tel: Telescope; PBS: polarization beam splitter; EDFA: erbium-doped optical fiber amplifier; AOM: acousto-optic modulator; and BPD: balanced photodetector.

and $J_n(\beta)$ $(n = 0, 1)$ is the nth-order Bessel function of the first kind. In (1), only the optical carrier and ±first-order optical sidebands are considered by assuming small signal modulation. As shown in Fig. 1(b), the optical carrier is along the +45° polarization direction, while the +first-order optical sideband is along the −45° polarization direction. The −first-order optical sideband is not shown in Fig. 1(b) because it will not be used in the measurement of velocity and depolarization ratio and will not affect the performance of the system.

Backscattered from the atmosphere, the dual-polarization light beam may suffer from the depolarization effect due to the polyhedral particles [12], so that the polarization state of the dual-polarization light beam is changed, which is given by

$$\mathbf{E}_B(t) \propto \frac{A_{\text{in}}}{\sqrt{2}} e^{j(\omega_c+\omega_d)t} \times \begin{bmatrix} (\sqrt{1-p})J_0(\beta) + \sqrt{p}J_1(\beta)(e^{j\omega_e t} - e^{-j\omega_e t}) \\ \sqrt{p}J_0(\beta) + (\sqrt{1-p})J_1(\beta)(e^{j\omega_e t} - e^{-j\omega_e t}) \end{bmatrix} \tag{2}$$

where p is the power proportion of the light whose polarization is changed from the copolarization direction to the cross-polarization direction, and ω_d is the Doppler frequency shift. As we can see in (2), both of the optical carrier and +first-order optical sidebands are presented along the ±45° polarization directions, which is shown in Fig. 1(c). In the receiver, one polarization component (taking the +45° as an example) is selected by a PBS and beats with the optical LO in a BPD. The electrical field of the optical LO can be written as

$$\mathbf{E}_{\text{LO}}(t) \propto A_{\text{LO}} e^{j(\omega_c+\omega_s)t} \tag{3}$$

where A_{LO} is the magnitude of the LO light, ω_s is the angular frequency of the modulation signal applied to the AOM. An electrical signal will be generated in the BPD, which is

given by

$$I(t) \propto A_{\text{in}}A_{\text{LO}}R[(\sqrt{1-p})J_0(\beta)\cos(\omega_s-\omega_d t)\infty + \sqrt{p}J_1(\beta)\cos(\omega_s-\omega_e-\omega_d t) - \sqrt{p}J_1(\beta)\cos(\omega_s+\omega_e-\omega_d t)] \quad (4)$$

where R is the responsibility of the BPD. By choosing suitable values of ω_s and ω_e, the frequency of the third term in (4) can be much higher than that of the first and the second terms so that it can be filtered out. The velocity can be extracted from the frequencies of the first and the second terms according to the Doppler Effect. Moreover, in (4), the first term is originated from the optical carrier and the second term is from the +first-order optical sideband. As a result, the first term is related to the copolarization backscattered light and the second term represents the cross-polarization backscattered component if only the backscattered light along the +45° polarization direction is detected. Because the depolarization ratio is extracted from the power ratio between the copolarization and cross-polarization backscattered lights [18], [19], it is reasonable to calculate the depolarization ratio p according to the intensity ratio of the first and the second terms in (4), given by

$$r = \frac{\sqrt{p}J_1(\beta)}{(\sqrt{1-p})J_0(\beta)} \quad (5)$$

$$p = \frac{[J_0(\beta)r]^2}{[J_0(\beta)r]^2+[J_1(\beta)]^2} = \frac{r^2}{r^2+r_0^2} \quad (6)$$

where r is the intensity ratio of the first and the second terms, $r_0 = J_1(\beta)/J_0(\beta)$, which can be measured in the calibration stage. Since the two single-frequency components are concurrent, the velocity and depolarization ratio can be simultaneously measured in real time.

III. Experiments and Discussion

An experiment is carried out to demonstrate the proposed polarization coherent Lidar system. A 1550-nm narrow linewidth LD [PureSpectrum (PS)-TNL] is used as the light source. One part of the light is modulated in a 40-Gb/s electrooptic PolM (Versawave, PL-40G-5-1550) by a 159-MHz RF signal. The other part is modulated at a fiber-coupled AOM (Gooch & Housego) by an 80-MHz RF signal to generate a frequency-shifted optical LO. In the receiver, a 2 × 2 3-dB fiber coupler is used to combine the backscattered light and the optical LO. The two output ports of the fiber coupler are connected to a BPD (Thorlabs PDB450C). The bandwidth of the BPD is 150 MHz. The output of the BPD is analyzed by an electrical spectrum analyzer (ESA, R&S FSV40). In addition, a high-resolution optical spectrum analyzer (OSA, APEX AP2040D) is employed to monitor the optical spectra.

Fig. 2 shows the optical spectra after the PolM. To evaluate the orthogonality of the optical carrier and sidebands, a PBS is inserted before the high-resolution OSA. The intensity of the optical carrier is much higher than that of the ±first-order optical sidebands along the +45° polarization direction (blue line), while along the −45-polarization direction (red line) the intensity of ±first-order optical sidebands are much higher than that of the optical carrier. The power ratio of the ±first-order optical sidebands along the two orthogonal polarization directions is around 25 dB, which might be restricted by the polarization extinction ratio of the PBS.

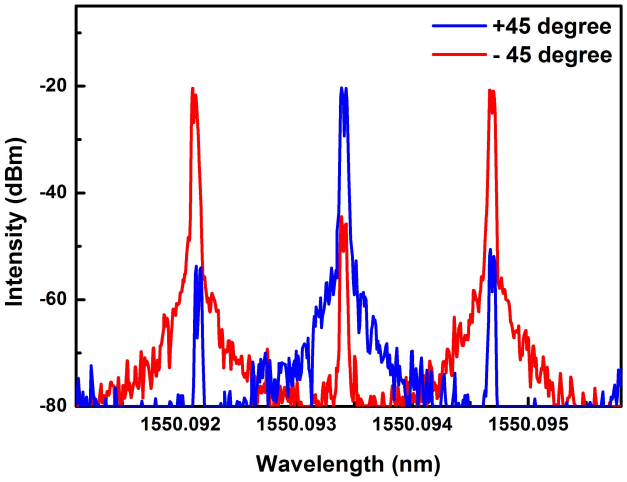

Fig. 2. Optical spectra of the dual-polarization light beam. Blue line: optical spectrum measured along the +45° polarization direction. Red line: optical spectrum measured along the −45° polarization direction.

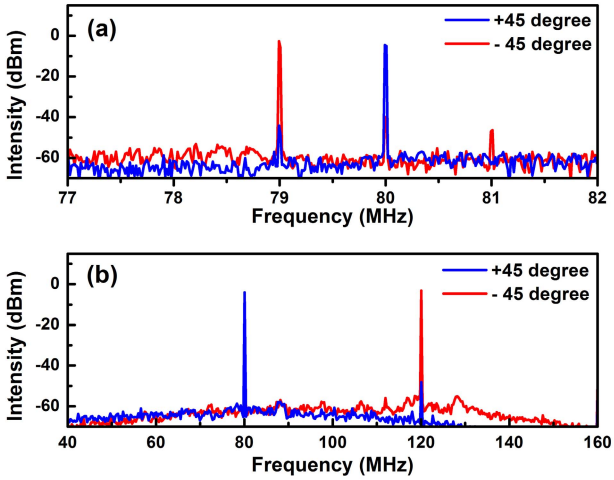

Fig. 3. Electrical spectra of the beat signals when the PBS in the receiver is configured to select the optical signal along the +45° polarization direction (blue line) or the −45° polarization direction (red line). There is not depolarization effect in the backscattered light. The modulation frequencies are set to (a) 159 MHz and (b) 200 MHz, respectively.

In the receiver, a PBS is used after the circulator (CL), so that only the backscattered light along one polarization direction (either the +45° or the −45°) beats with the frequency-shifted LO in the BPD. Fig. 3(a) shows the spectra of the beat signals. If there is no depolarization effect, cross-polarization component does not exist in the backscattered light. Only an 80-MHz (or 79-MHz) beat signal is generated when the optical signal along the +45° (or −45°) polarization direction is selected. The 3-dB bandwidth of the beat signal is limited by the resolution of the ESA, which is around 2 kHz. Cross-polarization signals can still be observed because of the limited polarization extinction ratio of the PBS. The intensities are more than 35 dB lower than the copolarization signal. It indicates that the minimum measurable depolarization ratio is less than 0.0003. Moreover, the frequency of the

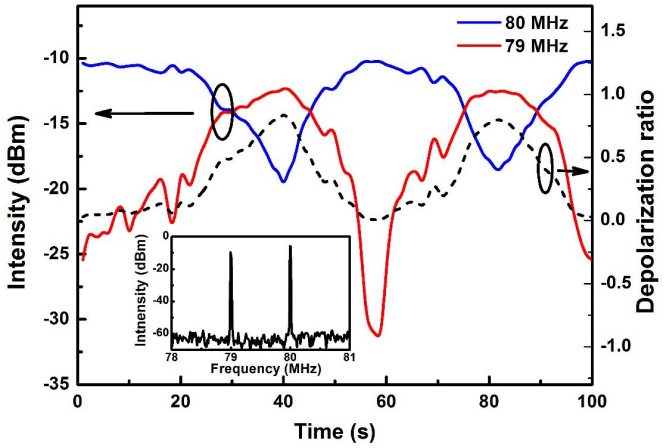

Fig. 4. Intensities of the 80- and 79-MHz frequency components when the PBS in the receiver is configured to select the optical signal along the +45° polarization direction during 100 s. The real-time depolarization ratio (black dashed line) is calculated from the measured intensities. Inset: the electrical spectrum of the beat signal.

driving signal for the PolM can be changed to measure targets with higher velocities (i.e., larger Doppler frequency shift). For example, we change the frequency from 159 to 200 MHz, and two beat signals at 80 and 120 MHz are observed in Fig. 3(b).

If the backscattered light is depolarized, there exists cross-polarization component, so both of the two single-frequency components can be observed when the optical signal along the +45° or −45° polarization direction is selected in the receiver. As we can see in the inset of Fig. 4, the beat signal along the +45°-polarization direction has two single-frequency components at 80 and 79 MHz, respectively. The 80-MHz component represents the copolarization backscattered light, while the 79-MHz one is from the cross-polarization component. The depolarization ratio can be calculated according to the intensity ratio between them. In the experiment, a depolarization plate is used, which is composed of two cemented quartz wedges. When a linearly polarized light passes through the plate at different positions, the polarization directions of the transmitted light are rotated by varying amounts. As a result, the polarization state of the backscattered light can be continuously changed by moving the depolarization plate. It is difficult to get the expected values of depolarization ratio at different positions of the plate, due to the fabrication-uncertainty of the plate. In the experiment, the depolarization of the backscattered light is measured according to the intensities of the two frequency components. The modulation index of the PolM is adjusted to let $r_0 = 1$. The intensities of the two frequency components are recorded over a period of 100 s. The recorded intensities of the 79- and 80-MHz components are shown as the red and blue lines in Fig. 4, respectively. The corresponding depolarization ratio can be calculated according to (6), which is shown as the dashed line in Fig. 4.

To demonstrate the simultaneous measurement of the depolarization ratio and the velocity in real time, a moving mirror is used as the target. The depolarization ratio of the backscattered light is continuously changed while the mirror

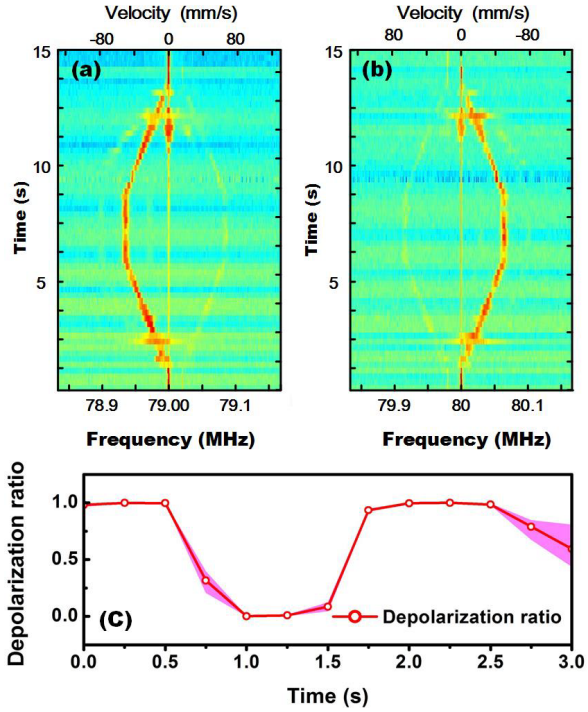

Fig. 5. Simultaneous measurement of the velocity and the depolarization ratio. (a) Component originated from the cross-polarization component. (b) Component originated from the copolarization component. (c) Calculated depolarization ratio during the uniform motion. The shadow presents the range of the calculated values at different frequencies.

is moving. First, the mirror moves forward with a constant acceleration of 10 mm/s^2 until the velocity reaches 50 mm/s. Then, the mirror moves forward with a constant velocity of 50 mm/s for 3 s followed by a deceleration section with acceleration of −10 mm/s^2. Fig. 5(a) and (b) show the spectra of two single-frequency components of the beat signal. The frequencies vary according to the velocity of the mirror due to the Doppler Effect. The frequency of the beat component originated from the optical carrier increases to 80.066 MHz during the uniform motion, while the frequency of the beat component originated from the +first-order optical sideband decreases to 78.934 MHz. The corresponding velocities are calculated, which can be read from the top axis in Fig. 5(a) and (b). The constant velocity of the mirror in the uniform motion section is calculated to be around 51.15 mm/s.

Except for the changes in the frequencies, both of the two single-frequency components show the continuous changes of intensity, since the backscattered light is depolarized during the motion. As we can see in Fig. 5(a) and (b), the intensities of the two frequency components show opposite changes. The depolarization ratio during the uniform motion section is calculated and shown in Fig. 5(c). The intensities at all frequencies within 3-dB bandwidth are recorded and used to calculate the depolarization ratio. The symbol and line are the mean value, and the shadow presents the range of calculated depolarization ratio. For practical measurements, the value of the depolarization ratio is around 0. In this condition, the measurement-uncertainty is relatively low. The frame rate of the measurement is 4 Hz, which is much higher than the

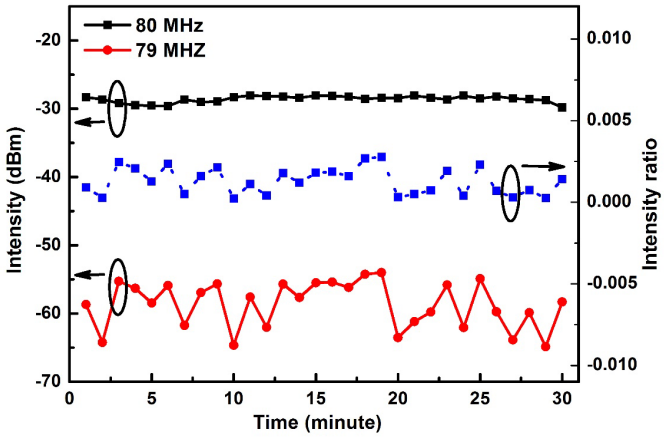

Fig. 6. Intensities of the two frequency components in the beat signal over a period of 30 min. Blue dashed line: calculated intensity ratio.

previous polarization Lidar [18]. The frame rate is limited by the ESA and can be further enhanced if it is replaced by a high-speed data acquisition card. It is notable that the two frequency components respectively originated from the copolarization and cross-polarization components are concurrent. As a result, the proposed polarization coherent Lidar system is able to implement a real-time measurement.

To verify the polarization stability of the Lidar, the intensities of the two frequency components in the beat signal are recorded over a period of 30 minutes in the condition of no depolarization effect. In Fig. 6, the intensities of the two frequency components remain stable during the measurement. The fluctuations in the intensity ratio are smaller than 0.003. To enhance the measurement sensitivity, a system with stable polarization states is required.

In the proposed Lidar, the depolarization ratio is defined as the power ratio between the copolarization and cross-polarization backscattered light, which was widely used in the previous Lidar system. However, the measurement does not isolate the optical rotation effect from the depolarization effect. The depolarization effect makes the light nonpolarized so that the optical power is equally distributed along all the polarization directions. On the other hand, the optical rotation effect only rotates the polarization direction of light, which is mainly caused by the Lidar system [24]. The electrical field of the rotated optical signal is projected on the two orthogonal polarization directions. In our proposed Lidar system, the depolarization effect and the optical rotation effect can be distinguished, if another BPD is adopted to detect the optical signal along the -45° polarization direction.

In that condition, the intensities of the beat signals can be given by

$$\begin{cases} I_1(t) \propto \sqrt{1-p_1-p_2} + \sqrt{\dfrac{p_1}{2}} + \sqrt{p_2}\cos\theta \\ I_2(t) \propto \sqrt{\dfrac{p_1}{2}} + \sqrt{p_2}\sin\theta \\ I_3(t) \propto \sqrt{1-p_1-p_2} + \sqrt{\dfrac{p_1}{2}} + \sqrt{p_2}\sin\theta \\ I_4(t) \propto \sqrt{\dfrac{p_1}{2}} + \sqrt{p_2}\cos\theta \end{cases} \tag{7}$$

where p_1 is the power proportion of the nonpolarized light, p_2 is power proportion of the polarization-rotated light, θ is the angle between the polarization direction of the rotated light and the $+45^\circ$ polarization direction. $I_1(t)$ and $I_2(t)$ are the beat signals originated from the backscattered light along the $+45^\circ$ polarization direction, while $I_3(t)$ and $I_4(t)$ are the beat signals originated from the backscattered light along the -45° polarization direction. The ratio between the intensities of the beat signals can be given by

$$\begin{cases} a_1 = c_1 \dfrac{\sqrt{\frac{p_1}{2}} + \sqrt{p_2}\sin\theta}{\sqrt{1-p_1-p_2} + \sqrt{\frac{p_1}{2}} + \sqrt{p_2}\cos\theta} \\ a_2 = c_2 \dfrac{\sqrt{1-p_1-p_2} + \sqrt{\frac{p_1}{2}} + \sqrt{p_2}\sin\theta}{\sqrt{1-p_1-p_2} + \sqrt{\frac{p_1}{2}} + \sqrt{p_2}\cos\theta} \\ a_3 = c_3 \dfrac{\sqrt{\frac{p_1}{2}} + \sqrt{p_2}\cos\theta}{\sqrt{1-p_1-p_2} + \sqrt{\frac{p_1}{2}} + \sqrt{p_2}\cos\theta} \end{cases} \tag{8}$$

where c_1, c_2, and c_3 are constant coefficients that can be obtained in the calibration. It is sufficient to obtain the values of p_1, p_2, and θ with the three equations in (8). As a result, the optical rotation effect and depolarization effect would be distinguished.

IV. Conclusion

We have proposed a compact all-fiber polarization coherent Lidar based on a PolM. Since the copolarization and cross-polarization backscattered lights are concurrent, the proposed Lidar system can implement simultaneous measurement of the velocity and depolarization ratio in real time. Moreover, since the copolarization and cross-polarization components produce beat signals with different frequencies, the Lidar does not require polarization-diversity transmitter or receivers to switch the polarization of light, making the system compact. An experiment is carried out. The velocity measurement error is around 2% and the depolarization ratio is simultaneously measured in real time. The minimum measurable depolarization is around 0.003, and the frame rate of the measurement is 4 Hz. The frame rate can be further enhanced using a high-speed data acquisition card. With a slight modification, the proposed polarization Lidar system can be used to distinguish the optical rotation effect and the depolarization effect.

References

[1] B. Journet and G. Bazin, "A low-cost laser range finder based on an FMCW-like method," *IEEE Trans. Instrum. Meas.*, vol. 49, no. 4, pp. 840–843, Aug. 2000.

[2] C. A. Northend, R. C. Honey, and W. E. Evans, "Laser radar (lidar) for meteorological observations," *Rev. Sci. Instrum.*, vol. 37, no. 4, pp. 393–400, Apr. 1966.

[3] R. C. Schnell *et al.*, "Lidar detection of leads in arctic sea ice," *Nature*, vol. 339, no. 4, pp. 530–532, Jun. 1989.

[4] B. Schwarz, "LIDAR: Mapping the world in 3D," *Nature Photon.*, vol. 4, no. 7, pp. 429–430, Jul. 2010.

[5] Y. Li, Y. Ruichek, and C. Cappelle, "Optimal extrinsic calibration between a stereoscopic system and a LIDAR," *IEEE Trans. Instrum. Meas.*, vol. 62, no. 8, pp. 2258–2269, Aug. 2013.

[6] R. T. Menzies and R. M. Hardesty, "Coherent Doppler lidar for measurements of wind fields," *Proc. IEEE*, vol. 77, no. 3, pp. 449–462, Mar. 1989.

[7] D. V. Vladutescu *et al.*, "Remote sensing instruments used for measurement and model validation of optical parameters of atmospheric aerosols," *IEEE Trans. Instrum. Meas.*, vol. 61, no. 6, pp. 1733–1746, Jun. 2012.
[8] J. Johansson, B. G. Marthinsson, and S. T. Eng, "Computer automation and error analysis of a CO_2-laser long-path absorption system for air pollution monitoring," *IEEE Trans. Instrum. Meas.*, vol. IM-27, no. 4, pp. 358–363, Dec. 1978.
[9] W. N. Chen, C. W. Chiang, and J. B. Nee, "Lidar ratio and depolarization ratio for cirrus clouds," *Appl. Opt.*, vol. 41, no. 30, pp. 6470–6476, Oct. 2002.
[10] A. Behrendt, T. Nakamura, and T. Tsuda, "Combined temperature lidar for measurements in the troposphere, stratosphere, and mesosphere," *Appl. Opt.*, vol. 43, no. 14, pp. 2930–2939, May 2004.
[11] R. M. Schotland, K. Sassen, and R. Stone, "Observations by lidar of linear depolarization ratios for hydrometeors," *J. Appl. Meteorol.*, vol. 10, no. 5, pp. 1011–1017, Oct. 1971.
[12] J. S. Tyo, D. L. Goldstein, D. B. Chenault, and J. A. Shaw, "Review of passive imaging polarimetry for remote sensing applications," *Appl. Opt.*, vol. 45, no. 22, pp. 5453–5469, Aug. 2006.
[13] S. Tan and R. M. Narayanan, "Design and performance of a multiwavelength airborne polarimetric lidar for vegetation remote sensing," *Appl. Opt.*, vol. 43, no. 11, pp. 2360–2368, Apr. 2004.
[14] J. E. Kalshoven and P. W. Dabney, "Remote sensing of the earth's surface with an airborne polarized laser," *IEEE Trans. Geosci. Remote Sens.*, vol. 31, no. 2, pp. 438–446, Mar. 1993.
[15] J. A. Shaw *et al.*, "Polarization lidar measurements of honey bees in flight for locating land mines," *Opt. Express*, vol. 13, no. 15, pp. 5853–5863, Jul. 2005.
[16] K. Sassen, "The polarization lidar technique for cloud research: A review and current assessment," *Bull. Amer. Meteorol. Soc.*, vol. 72, no. 12, pp. 1848–1866, Dec. 1991.
[17] N. Sugimoto *et al.*, "Observation of dust and anthropogenic aerosol plumes in the Northwest Pacific with a two-wavelength polarization lidar on board the research vessel Mirai," *Geophys. Res. Lett.*, vol. 29, no. 19, pp. 7-1–7-4, Oct. 2002.
[18] N. L. Seldomridge, J. A. Shaw, and K. S. Repasky, "Dual-polarization lidar using a liquid crystal variable retarder," *Opt. Eng.*, vol. 45, pp. 1234–1237, Oct. 2006.
[19] C. J. Flynna, A. Mendozaa, Y. Zhengb, and S. Mathurb, "Novel polarization-sensitive micropulse lidar measurement technique," *Opt. Express*, vol. 15, no. 10, pp. 2785–2790, Mar. 2007.
[20] S. Kameyama, T. Ando, K. Asaka, Y. Hirano, and S. Wadaka, "Compact all-fiber pulsed coherent Doppler lidar system for wind sensing," *Appl. Opt.*, vol. 46, no. 11, pp. 1953–1962, Apr. 2007.
[21] C. F. Abari, A. T. Pedersen, and J. Mann, "An all-fiber image-reject homodyne coherent Doppler wind lidar," *Opt. Express*, vol. 22, no. 21, pp. 25880–25894, Oct. 2014.
[22] C. F. Abari, X. Chu, R. Michael Hardesty, and J. Mann, "A reconfigurable all-fiber polarization-diversity coherent Doppler lidar: Principles and numerical simulations," *Appl. Opt.*, vol. 54, no. 30, pp. 8999–9009, Oct. 2015.
[23] C. Wang *et al.*, "1.5 μm polarization coherent lidar incorporating time-division multiplexing," *Opt. Express*, vol. 25, no. 17, pp. 20663–20674, Aug. 2017.
[24] M. Hayman and J. P. Thayer, "Explicit description of polarization coupling in lidar applications," *Opt. Lett*, vol. 34, no. 5, pp. 611–613, Mar. 2009.
[25] S. Pan and Y. Zhang, "Tunable and wideband microwave photonic phase shifter based on a single-sideband polarization modulator and a polarizer," *Opt. Lett.*, vol. 37, no. 21, pp. 4483–4485, Nov. 2012.
[26] A. L. Campillo, "Orthogonally polarized single sideband modulator," *Opt. Lett.*, vol. 32, no. 21, pp. 3152–3154, Nov. 2007.
[27] Y. Zhang and S. Pan, "Broadband microwave signal processing enabled by polarization-based photonic microwave phase shifters," *IEEE J. Quantum Electron.*, vol. 54, no. 4, pp. 1–12, Aug. 2018, Art no. 0700112.

Zhongyang Xu received the B.S. degree in physics from Sun Yat-sen University, Guangzhou, China, in 2010, and the Ph.D. degree in physics from Tsinghua University, Beijing, China, in 2015.

He is currently a Lecturer with the Key Laboratory of Radar Imaging and Microwave Photonics, Ministry of Education, Nanjing University of Aeronautics and Astronautics, Nanjing, China. His current research interests include frequency-modulated continuous-wave (FMCW) detection and microwave photonics measurement.

Hongxiang Zhang received the B.S. degree in optical engineering from Jiangsu Normal University, Xuzhou, China, in 2017. He is currently pursuing the M.S. degree with the Key Laboratory of Radar Imaging and Microwave Photonics, Ministry of Education, Nanjing University of Aeronautics and Astronautics, Nanjing, China.

His current research interests include lidar detection and microwave photonics measurement.

Kai Chen received the B.S. degree from the Nanjing University of Aeronautics and Astronautics, Nanjing, China, in 2018, where he is currently pursuing the M.S. degree with the Key Laboratory of Radar Imaging and Microwave Photonics, Ministry of Education.

His current research interests include microwave photonics measurement.

Shilong Pan (S'06–M'09–SM'13) received the B.S. and Ph.D. degrees in electronics engineering from Tsinghua University, Beijing, China, in 2004 and 2008, respectively.

From 2008 to 2010, he was a Vision 2010 Post-Doctoral Research Fellow with the Microwave Photonics Research Laboratory, University of Ottawa, Ottawa, ON, Canada. In 2010, he joined the College of Electronic and Information Engineering, Nanjing University of Aeronautics and Astronautics, Nanjing, China, where he is currently a Full Professor and the Deputy Director of the Key Laboratory of Radar Imaging and Microwave Photonics, Ministry of Education. He has authored or coauthored more than 390 research papers, including more than 210 papers in peer-reviewed journals and 180 papers in conference proceedings. His current research interests include microwave photonics, which includes optical generation and processing of microwave signals, analog photonic links, photonic microwave measurement, and integrated microwave photonics.

Dr. Pan is a fellow of IET and SPIE, and a Senior Member of OSA. He is also a Steering Committee Member of the IEEE International Topical Meeting on Microwave Photonics, the International Conference on Optical Communications and Networks, and the International Conference on Information Optics and Photonics. He is also a Technical Committee Member of IEEE MTT-3 Microwave Photonics. He was selected to receive an OSA Outstanding Reviewer Award in 2015 and as a Top Reviewer of the IEEE/OSA JOURNAL OF LIGHTWAVE TECHNOLOGY in 2016. He was a recipient of the Scientific and Technological Innovation Leading Talents Award of the National Ten Thousand Plan in 2018. He has also served as a chair for a number of international conferences, symposia, and workshops, including the TPC Chair of the International Conference on Optical Communications and Networks in 2015 and the TPC Co-Chair of the IEEE International Topical Meeting on Microwave Photonics in 2017. He is currently an Associate Editor of *Electronics Letters* and a Topical Editor of *Chinese Optics Letters.*